COUPLING BETWEEN FLEXIBLE SHIP AND LIQUID SLOSHING USING POTENTIAL FLOW ANALYSIS AND ITS EFFECT ON WAVE-INDUCED LOADS

Y B Lee[1, 2], M Tan[1], P Temarel[1] & S H Miao[1]

(1) Ship Science, School of Engineering Sciences, University of Southampton, UK
(2) Daewoo Shipbuilding & Marine Engineering, Co. Ltd., Korea

SUMMARY

In this paper the potential flow approach adopted in previous investigations for the coupling effect between rigid body ship motion and sloshing is extended to the flexible ship-partially filled tank system, using the de-singularised Rankine source method. The unified method is verified by applying it to the sloshing in a partially filled rectangular tank with a flexible wall. The main aim of this paper is to investigate the influence of hull flexibility on the hydrodynamic forces and moments associated with liquid sloshing and the effect of sloshing on wave-induced responses. The coupling effect between flexible ship and sloshing is illustrated for an idealized LNG carrier in beam regular waves, considering different partial filling scenarios. Symmetric and antisymmetric responses, such as bending and torsional moments, in beam regular waves are investigated with and without coupling effect from liquid sloshing. From the limited numerical comparisons, it is found that liquid sloshing has an influence on the response of distortional as well as rigid modes, i.e. wave-induced motions and loads.

NOMENCLATURE

$\boldsymbol{A}_h$	Generalised added mass matrix of hull
$\boldsymbol{A}_{sl}$	Generalised added mass matrix due to liquid in partially filled tanks
$\boldsymbol{a}_h$	Generalised mass matrix of hull
$\boldsymbol{B}_h$	Generalised fluid damping matrix of hull
$\boldsymbol{b}_h$	Generalised structural damping matrix of hull
$\boldsymbol{C}_h$	Generalised fluid restoring matrix of hull
$\boldsymbol{C}_{sl}$	Generalised fluid restoring matrix due to liquid in partially filled tanks
$\boldsymbol{c}_h$	Generalised stiffness matrix of hull
$\boldsymbol{n}$	Normal vector on tank boundaries
$\boldsymbol{p}$	Principal coordinate vector
p_r	Amplitude of r^{th} principal coordinate
r	Index for global mode shape of hull
t	Time (s)
$\boldsymbol{u}_r$	In vacuo (dry) mode shape for global distortions of hull
$\boldsymbol{\Xi}$	Generalised wave excitation vector of hull
φ_r	Velocity potential associated with r^{th} mode
ω_{mn}	Natural frequency of liquid sloshing in partially filled tank(rad s^{-1})
ω_r	Natural frequency of hull (rad s^{-1} or Hz)
ω_e	Encounter frequency (rad s^{-1})

1. INTRODUCTION

The demand for building Liquefied Natural Gas (LNG) carriers has dramatically increased since the early 2000s and this trend is likely to continue for a relatively long period since many countries consider natural gas as their future energy supply. One of the design issues for LNG carriers is the sloshing phenomenon, as containment systems widely used nowadays do not have internal structures. In addition, there is a huge demand for much larger LNG vessels in order to maximise profit. Furthermore, the demand for operations in partially filled condition inevitably increases the possibility of sloshing. As a consequence, many investigations have been carried out to predict sloshing loads and the responses of hull and containment system in order to ensure structural integrity of the whole system [e.g. 1, 2].

Investigation of the interaction effects between ship's rigid body motions and sloshing loads is of particular interest. This is of practical benefit not only for local structural design due to sloshing but also for global ship design. Ship motion performance is considered very critical in ship to ship transfer of liquid cargo and also in some offshore structures such as FPSOs, where a large number of process modules are installed at various deck levels. Therefore, good prediction of coupling effects between sloshing loads and ship motions are critical for the design of marine/offshore structures.

Recent strong interest along with enhanced computational capability resulted in a systematic analysis of the coupling between sloshing and ship motions numerically, both in frequency and time domains, as well as experimentally. For example, Rognebakke & Faltinsen [3] carried out nonlinear sloshing analysis in time domain and experimentation for two-dimensional problems. Kim [4] and Nam et al [5] investigated the three-dimensional problem in the time domain. The three-dimensional problem was investigated by Malenica et al [6] and Newman [7] in the frequency domain. Molin et al [8] and

Nasar et al [9] carried out experiments on a barge with partially-filled tanks.

It is noted that the vast majority of these activities are mainly concerned with coupling between rigid ship motions and sloshing loads. However, due to the fact that larger size ships are on demand and already being built, more effort needs to be focused on the interaction between the ship, globally treated as a flexible structure, and liquid cargo in tanks. This is because as LNG carrier dimensions increase the overall stiffness of the ship decreases resulting in relatively low resonance frequencies associated with global distortions, which are within or close to the range of significant wave energy and excitation. Furthermore this decrease in resonance frequencies associated with global distortions results in bringing them closer to sloshing resonance frequencies, i.e. natural frequencies of the liquid inside the partially filled tank.

Lee et al also developed a method, whereby forces and moments due to sloshing are presented using added mass coefficients, to model the coupling between rigid body motions and sloshing [10 - 12]. This method employed source distribution (i.e. pulsating or Rankine source) on the boundaries and, when required the mean free surface, of the tank. This method was verified through comparisons with experimental measurements [8], analytical values [13] and other available numerical predictions [6, 14]. Subsequently the de-singularised Rankine approach was extended to generate a unified method for predicting the fluid-structure interactions of a coupled flexible ship – partially filled tank(s) system [15]. There are no experimental measurements or other numerical predictions against which the unified method can be compared. Therefore, in this paper, the results of a verification study for sloshing in a partially filled tank with one flexible wall are presented. Predicted added mass values of a submerged flexible plate are compared with other available numerical predictions [16, 17]. The main focus of the paper is on predicting the responses of an idealized LNG carrier stationary in beam regular waves, considering three partial filling scenarios. The influence of liquid sloshing on wave-induced loads, such as vertical and horizontal bending, and torsional moments is illustrated.

2. THEORETICAL BACKGROUND

2.1 SLOSHING

A potential flow analysis was previously used for the coupling between ship rigid motions and liquid sloshing in a tank(s). In these investigations the pulsating source Green's function and the conventional and de-singularised Rankine source approaches were used for the evaluation of the hydrodynamic actions due to liquid sloshing inside a partially filled rigid tank [10, 11]. The de-singularised Rankine approach was selected, due to its advantages in terms of accuracy and efficiency, for application to liquid inside a partially filled tank subject to the global distortions of a flexible ship [12, 15]. The process is a unified or generalized one, namely it encompasses rigid body motions and distortions. The velocity potential of the Rankine source satisfies Laplace's equation, the linearised free surface condition and body boundary condition shown in equation1, namely

$$\begin{aligned} &\nabla^2\varphi_{\mathrm{r}} = 0 && \text{in the liquid domain} \\ &-\frac{\omega_{\mathrm{e}}^2}{g}\varphi_{\mathrm{r}} + \frac{\partial\varphi_{\mathrm{r}}}{\partial z} = 0 && \text{on mean free surface} \\ &\frac{\varphi_r}{\partial \boldsymbol{n}} = i\,\omega_e(\boldsymbol{u}_r.\boldsymbol{n}) && \text{on wetted tank boundaries, } \bar{S} \end{aligned} \tag{1}$$

where φ_{r} denotes the radiation potential (r=1 surge, r=2 sway, r=3 heave, r=4 roll, r=5 pitch, r=6 yaw, r=7, 8,… distortions), $\boldsymbol{u}_{\mathrm{r}}=\{\mathrm{u},\ \mathrm{v},\ \mathrm{w}\}_{\mathrm{r}}$ the rth mode shape, $\boldsymbol{n}$ the normal vector and ω_{e} the oscillation or wave encounter frequency.

In the de-singularised Rankine source method sources are located outside the liquid domain, but the body and free surface boundary conditions are applied on the actual tank boundaries and mean free surface. These are discretised using four-cornered panels. This is achieved through the offset $\varepsilon=(\mathrm{OF}\ S^{1/2})$, where OF is the offset factor and S the panel area [11, 12]. Once the velocity potential is obtained the relevant generalized added mass, with reference to an axis system whose origin is on the free surface of the tank, is obtained as

$$A_{rk} = (\rho/\omega_{\mathrm{e}}^2)\,\Re\iint_{\bar{S}} \boldsymbol{n}^{\mathrm{T}}\,\boldsymbol{u}_{\mathrm{r}}(i\,\omega_{\mathrm{e}})\varphi_{\mathrm{k}}\,d\bar{S} \tag{2}$$

where ρ denotes the density of the liquid in the tanks. A free surface correction when the tank has a vertical movement, as suggested by Malenica et al [6], is extended to the generalized method of partially filled tanks in a flexible ship.

For the coupling between flexible ship and liquid sloshing, global distortions of the ship are used for satisfying the body boundary condition for sloshing analysis. Generalized unit mass matrix is used for normalisation because it is more convenient when data is transferred from commercial FE codes. An interpolation scheme is used to obtain distortions at tank boundaries from the modal distortions of the FE model, allowing for independence between FE model and panel idealization of the free surface and boundaries of the tank.

For a rectangular tank natural frequencies associated with the liquid sloshing inside the tank can be obtained according to Graham & Rodriguez [13], namely

$$\omega_{\mathrm{mn}}^2 = g\,k_{\mathrm{mn}}\tanh(k_{\mathrm{mn}}\,T) \tag{3}$$

where m and n denote the modes in longitudinal and transverse directions, respectively, T the depth of liquid inside the tank and

$$k_{\mathrm{mn}} = \pi\sqrt{\frac{(2\mathrm{m}+1)^2}{L^2} + \frac{(2\mathrm{n}+1)^2}{B^2}},$$

with L and B denoting the length and breath of the tank and m, n=0, 1, 2, etc. It should be noted that for longitudinal modes the second term is omitted and for transverse modes the first term is omitted.

2.2 GENERALISED COUPLED EQUATIONS OF MOTION

The generalized equations of motion for a flexible ship – partially filled tank(s) system travelling in regular waves are

$$(\boldsymbol{a}_{\mathrm{h}} + \boldsymbol{A}_{\mathrm{h}} + \boldsymbol{A}_{\mathrm{sl}})\ddot{\boldsymbol{p}} + (\boldsymbol{b}_{\mathrm{h}} + \boldsymbol{B}_{\mathrm{h}})\dot{\boldsymbol{p}} + (\boldsymbol{c}_{\mathrm{h}} + \boldsymbol{C}_{\mathrm{h}} + \boldsymbol{C}_{\mathrm{sl}})\boldsymbol{p} = \boldsymbol{\Xi}\exp(i\omega_{\mathrm{e}}t) \quad (4)$$

This system of equations has the form developed by Bishop et al [18] for fluid-flexible hull interaction. Terms to allow for the effects of sloshing are added, based on the analysis by Malenica et al and Lee et al [6, 10, 11, 15]. In these equations $\boldsymbol{a}_{\mathrm{h}}$ and $\boldsymbol{c}_{\mathrm{h}}$ denote the hull's generalized mass and stiffness matrices, obtained from dry hull analysis and including the mass of the liquid in the tanks treated as a frozen mass. $\boldsymbol{b}_{\mathrm{h}}$ is the generalized structural damping matrix, assumed diagonal. $\boldsymbol{A}_{\mathrm{h}}$ and $\boldsymbol{B}_{\mathrm{h}}$ denote the encounter frequency dependent generalized added mass and fluid damping of the hull at a draught which accounts for the liquid in the tanks treated as frozen mass. $\boldsymbol{C}_{\mathrm{h}}$ is the corresponding generalized fluid restoring matrix and $\boldsymbol{\Xi}$ the wave excitation vector, comprising incident wave and diffraction components. Furthermore, $\boldsymbol{p}(t)=\boldsymbol{p}\exp(i\omega_{\mathrm{e}}t)$, $\dot{\boldsymbol{p}}(t)$, $\ddot{\boldsymbol{p}}(t)$ denote the principal coordinate vector and its derivatives. $\boldsymbol{A}_{\mathrm{h}}$, $\boldsymbol{B}_{\mathrm{h}}$ and $\boldsymbol{\Xi}$ were evaluated using the three-dimensional hydroelasticity theory developed by Bishop et al [18], using a distribution of pulsating sources over the mean wetted surface of the hull.

$\boldsymbol{A}_{\mathrm{sl}}$ denotes the frequency dependent generalized added mass matrix due to the liquid in the tanks, suitably transformed to the axis system used for ship motions and distortions, namely the equilibrium axes. Lee et al discussed the trends of these added mass values as the frequency approaches zero [10, 11, 15]. Allowance has to be made so that the "zero frequency" values, e.g. the frozen liquid mass and inertia, are not accounted twice. This allowance is extended to all modes, under the assumption that as the frequency tends to zero there should be no influence due to liquid sloshing in the tank(s). These effects are included when using the generalized added masses of equation 2 to generate the $\boldsymbol{A}_{\mathrm{sl}}$ matrix. It should be noted that $\boldsymbol{C}_{\mathrm{sl}}$ only contains corrections associated with rigid body modes, allowing for the influence of free surface on the roll and pitch restoring moments.

3. VERIFICATION

3.1 COUPLING BETWEEN RIGID BODY MOTIONS AND SLOSHING

Lee et al, in their previous investigations, compared predictions obtained using potential flow analysis to model the coupling between rigid body motion and liquid sloshing in a partially filled tank with other available results [10, 11]. For example they compared added mass (or inertia) due to liquid in a partially filled rectangular tank, predicted using pulsating and conventional and de-singularised Rankine source methods, with analytical solution [13], the Rapid Sloshing Model (RSM) [14] and another potential flow analysis [6]. In addition Lee et al simulated the experiments carried out by Molin et al [8] involving a rectangular barge stationary in beam regular waves, carrying a partially filled rectangular tank. Comparison of predicted roll motion with results from RSM and experimental measurements indicated that the method developed is capable of modelling the coupling effect between sloshing liquid and rigid ship [11]. A further investigation was carried out using the de-singularised Rankine method to predict the sway motion corresponding to the experiments carried out by Rognebakke & Faltinsen [3] for one- and two-tank configurations. These comparisons also indicated good overall agreement [12].

In addition the unified approach developed for evaluating added mass values due to liquid in partially filled tank, subject to the global distortions of a hull, was initially verified through comparisons of the rigid body added mass values [12, 15].

3.2 SLOSHING DUE TO A FLEXIBLE TANK WALL

The unified method outlined in section 2 was applied to a partially filled rectangular tank with one flexible wall (i.e. plate), investigated by Lee and Kim et al [16, 17], in order to verify the accuracy of the numerical procedures developed in the presence of distortions. The tank used is shown in Figure 1, where L=l=1m, B=b=0.25m, h=0.6m and T=0.3m i.e. 50% filling condition. The flexible wall, shown panelled in Figure 1, is made of 1.4mm aluminium, whilst all other tank boundaries are made of 20mm flexiglass and assumed to be rigid. The flexible wall is assumed to be clamped at all its boundaries.

The first few natural frequencies of the flexible wall when the tank is empty (i.e. dry case), evaluated using the NASTRAN FE software, are shown in Table 1. The corresponding (dry) mode shapes of the flexible wall can be evaluated using the mode summation method applied to a rectangular plate clamped on all sides [16, 17, 19]. In the description of the modes shown in Table 1, (p, q) denote the number of half waves in the vertical and transverse directions of the flexible wall, respectively. The velocity distribution on the submerged part of the

dry flexible wall is shown in Figure 2, for the 1st mode shape, i.e. (1, 1). This, as expected, shows symmetry about the centre of the wall, situated at the liquid free surface for the 50% filling condition considered.

Lee, and Kim et al showed that the hydrodynamic actions associated with sloshing due to the flexible wall can be expressed in the form of added mass coefficients of a partially submerged plate [16, 17]. As the natural frequencies of the submerged flexible wall are much higher than the natural frequencies associated with the liquid sloshing inside the tank, the linear free surface boundary condition, given in equation 1, was further simplified to φ_r=0. These added mass coefficients are included when evaluating the natural frequencies of the flexible wall (plate) when the tank is partially filled, i.e. the wet case. The wet natural frequencies are shown in Table 1, together with predictions from the NASTRAN FE software also using the added mass through the MFLUID option [17]. As expected the wet natural frequencies are much lower than the dry natural frequencies. The first few wet modes, corresponding to the wet natural frequencies in Table 1, are shown in Figure 3, clearly illustrating the effect of submergence.

The rectangular tank, shown in Figure 1, was discretized using 24, 6 and 7 panels in the longitudinal, transverse and vertical directions, respectively, for the 50% filling case. In the first instance the simplified free surface boundary condition, φ_r=0, was applied. Using the generalised added mass values obtained, the calculated wet natural frequencies are also shown in Table 1. Comparison of the wet natural frequencies predicted by the different methods shown in Table 1, demonstrates good agreement, except for small differences for the 4th mode, i.e. (4, 1). This indicates that the current method is providing accurate predictions for the added mass of a flexible partially submerged plate.

The pressure distribution (obtained using φ_r=0) in the liquid domain of the rectangular tank, corresponding to the 1st wet mode is shown in Figure 4. This looks very similar to the first mode shape shown in Figure 3, with the peak pressures on the flexible wall occurring above the centre of the submerged part of the wall. It can also be seen in Figure 4 that the fluid region affected by the submerged oscillating wall is rather limited. Subsequently the current method was applied using the linearised free surface condition given in equation 1. The variation of the generalised added mass for the 1st mode with frequency is shown in Figure 5. As can be seen there are many peaks associated with the natural frequencies of the liquid sloshing inside the tank. As the frequency increases the generalised added mass tends to the asymptotic value obtained from the φ_r=0 solution [12]. The pressure distribution for the first mode shape at an excitation frequency of 9.6 rad/s, the 2nd antisymmetric resonance for liquid sloshing inside the tank, is shown in Figure 6. This figure clearly shows the development of a, longitudinally, antisymmetric wave pattern along the tank. On the other hand for higher excitation frequencies, e.g. 30 rad/s, the pressure distribution obtained is very similar to that shown in Figure 4 [12]. This demonstrates the importance of not simplifying the linearised free surface condition in the relatively low frequency range.

4. APPLICATION TO AN IDEALIZED LNG CARRIER

The analysis outlined in section 2 is applied to an idealized LNG carrier stationery in beam regular waves, considering various scenarios with partially filled tanks. The principal particulars of the LNG carrier are given in Table 2. They correspond to a real LNG carrier, of 200000 m^3 capacity, and of same length, breadth, depth and displacement. The shape of the hull is assumed rectangular, for simplicity of application, and is divided into 5 tanks of 63m length each as shown in Figure 7. Three filling scenarios are considered: (A) Tank 1 (situated at the bow) alone, (B) Tank 3 (situated either side of amidships) alone and (C) all tanks, acting as one tank for the whole ship. In each scenario the tank is filled to a depth T=20 m, i.e. 74% filling level. The total displacement of the idealized LNG carrier is maintained at a constant value of 142500 tonnes for all the scenarios considered. For scenario C the LNG mass is 124740 tonnes, all treated as liquid. For scenarios A and B the liquid LNG mass in the partially filled tank is 24948 tonnes, with the remainder of the LNG mass treated as frozen. This treatment may appear unrealistic, but it was implemented in order to perform comparison of the responses without having to account for variations in total mass and inertia. It also allows the use of the same FE structural model for all three scenarios, using a uniform mass distribution.

4.1 DRY AND WET ANALYSES - UNCOUPLED

The FE model of the idealized LNG carrier, comprising 6522 shell elements in total, is shown in Figure 7. It has double skin on the sides, but only single bottom. The deck plating in the idealized LNG carrier is not shown, to enable internal view. Furthermore, the fictitious transverse bulkheads used, as per previous practice [20], in order to avoid local distortions are also not shown in Figure 7.

The dry hull or in vacuo natural frequencies for the first five modes are shown in Table 3. These are of the same order of magnitude as those estimated for the real ship. This set of mode shapes, comprising two vertical bending (VB), two horizontal bending (HB) and one twisting (T) mode, is ideal for illustrating this application for both symmetric and antisymmetric dynamic behaviour, though the latter is much more important in the beam regular waves investigated. It should be noted that, as the idealized LNG carrier is a closed box, there is no

coupling between the antisymmetric distortions of horizontal bending and torsion.

A selection of generalized added masses corresponding to the distortion modes, A_{77} (2-node vertical bending), A_{88} (2-node horizontal bending) and A_{99} (1-node twisting), for the idealized LNG carrier oscillating in water, i.e. liquid mass in tanks treated as frozen (or uncoupled case), are shown in Figure 8. These were obtained using a relatively crude 338 panel idealization of the LNG carrier's mean wetted surface. These can be useful in comparing the magnitudes of the generalized added masses due to liquid in partially filled tank(s), shown in Figure 9. The principal coordinate amplitudes of the LNG carrier, liquid mass in tanks treated as frozen (or uncoupled case) will be discussed later and are shown in Figure 12.

4.2 SLOSHING HYDRODYNAMICS

Before examining the numerically predicted generalised added mass values, it is important to calculate the natural frequencies associated with liquid sloshing for scenarios A (or B) and C, evaluated using equation 3 These are shown in Table 4 for the first few modes corresponding to longitudinal, transverse and diagonal waves.

For the numerical predictions the walls, bottom and free surface of the tank were idealised using a total of 376 and 1496 panels, for scenarios A (or B) and C, respectively. A selection of generalized added masses, i.e. elements of matrix $\boldsymbol{A}_{sl}$, are shown in Figures 9 and 11 for all three scenarios. Please note that the added mass values in Figures 9 and 11 are for density ρ=1000 kg/m3. When these are incorporated into equation 4 they are modified to account for LNG density ρ=450 kg/m3. All added masses are with reference to the equilibrium axis system of the hull, located at the LCG.

The influence of the sloshing natural frequencies, shown in Table 4, can be seen on the generalised added masses shown in Figures 9 and 11. For example the 1st transverse natural frequency (0.79 rad/s) results in troughs and peak for A_{88} in Figure 9, for scenarios A, B and C, respectively. The same effect can be seen for the generalised added masses A_{22} and A_{82}, shown in Figure 11. The effect of the 2nd transverse mode (1.45 rad/s) can also be noted in A_{88} of Figure 9 and A_{22} and A_{82} of Figure 11, although it is rather small. Similarly the effect of the 1st diagonal mode (in the vicinity of 0.8 or 0.9 rad/s) can be seen on A_{99} in Figure 9. For all scenarios considered. Finally the effect of the longitudinal modes can be seen in A_{77} in Figure 9, for scenario C (in the vicinity of 0.4 rad/s) and to a lesser extent for scenarios A and B (in the vicinity of 0.6 rad/s).

The generalised added masses due to sloshing corresponding to distortions, shown in Figures 9 and 11 are affected mainly by the dimensions of the tank, as can be seen by comparing scenarios A and B with scenario C. However, the position of the tank can also have an important effect, depending on the mode shape. This can be observed by comparing scenarios A and B, with same tank dimensions but different position along the ship. For example A_{77} and A_{88}, in Figure 9, show small differences between scenarios A and B. The same is true for the sway added mass A_{22}, shown in Figure 11. On the other hand A_{99}, shown in Figure 9, and the cross coupling added mass A_{82}, shown in Figure 11 display larger differences between scenarios A and B.

Comparing Figures 8 and 9 one can see that, in general, the magnitudes of the generalized masses for the distortion modes are of same order, for the uncoupled ship and sloshing scenarios. Understanding the interaction between hull motions and distortions, i.e. the mode shapes and direction of sloshing loads is important in explaining the extent of coupling. For example, symmetric modes (e.g. 2-node VB) will not result in significant sloshing loads in the longitudinal direction, even when considering scenario C. This will result in weak coupling between the elements of the symmetric mode shapes, rigid or distortional, of A_{sl}. On the other hand, this is not the case for the antisymmetric modes, as illustrated in Figure 11. Comparing scenarios B and C, as shown in Figure 10, one notes that scenario C results in much larger values for A_{22}, especially at resonance, as one would physically expect. Furthermore, the partial filling scenario also affects the coupling. For example in scenario C the distribution of the sway force is such that it decreases the influence of the two-node horizontal bending mode, whilst for scenario A or B this influence is more pronounced. This can be clearly seen from the values of A_{82}, shown in Figure 11. These and other examples, not included in the paper, show that the method adopted provides results which are qualitatively right [12].

4.3 WET HULL ANALYSIS - COUPLED

A selection of the amplitudes of the principal coordinates of the idealized LNG carrier stationary in beam regular waves, for partial filling scenarios A, B and C, as well as for the case where the liquid is treated as frozen, denoted as "uncoupled" are shown in Figure 12. These are evaluated from equation 4, using the appropriate values for the elements of the matrices involved. As the interest of this paper is focused on wave-induced loads, only principal coordinates for the distortion modes are shown. The rigid body principal coordinates were discussed by Lee et al [15]. Zero values were used for the structural damping component, in order to exclude its influence from the responses when comparing the uncoupled case with scenarios A, B and C.

For the symmetric motions, heave, as expected, will result in negligible differences between all cases considered [12]. This is also true for the symmetric distortional principal coordinate amplitudes. For example one notes that for p_7, shown in Figure 12, there is very little difference between all three partial filling scenarios and the uncoupled case up to about 2 rad/s. The wet

resonance frequency associated with the 2-node VB distortion is around 2.5 rad/s. In this vicinity there appear to be some differences between the various scenarios. Whilst the uncoupled case and scenario A show sharp peaks at this wet resonance, the peaks appear much smaller for scenarios B and C. The same type of behaviour is displayed by principal coordinate p_{10}, the 2nd symmetric distortional mode [12]. This aspect may require further investigation, as it may be important in terms of springing and whipping.

For the antisymmetric distortions the amplitude for p_8, the 2-node HB mode, is much larger for scenarios A and B in the vicinity of 1 rad/s compared to the uncoupled case and scenario C. This is a result of significant coupling between sway (mode r=2) and roll (mode r=4) and mode r=8, which was discussed in section 4.2. The consequences will be that the resultant horizontal bending moment will have much larger values for partially filled cases similar to scenarios A and B compared to the uncoupled case. This aspect may require further verification in terms of additional scenarios, even though normal operational conditions do not allow for one tank to be partially filled in beam seas. For scenario C, i.e. whole ship partially filled, the magnitudes of p_8 are of similar order as those of the uncoupled case, though the occurrence of peaks is influenced by sloshing resonances. On the other hand the amplitude of p_{11}, 3-node HB mode, is very similar for scenarios A, B and the uncoupled case, in the vicinity of 0.5 rad/s, but there is a large peak in the vicinity of 1 rad/s for scenario A. This shows the complexity of the interactions between different modes influenced by the filling scenario. All cases behave in a similar manner in the vicinity of the wet resonance frequencies associated with modes r=8 and r=11, for both p_8 and p_{11}.

There is very little difference between scenarios A and B in the vicinity of the first peak, for the amplitude of p_9 the first twisting mode, which is slightly larger than that of the uncoupled case. However, the difference between scenarios A and B around 1 rad/s is pronounced, with scenario A displaying a substantial peak. This is attributed to the more significant contributions from mode r=9, 1-node twisting, for scenario A. Scenario C has the smallest peak values, similar to the behaviour of p_8 and p_{11}.

Wave-induced loads, either symmetric or antisymmetric, for all case considered, are obtained by summing the product of principal coordinate and modal internal action for each distortional mode. For example the vertical bending moment, $M_y(x,t)$, in regular waves is expressed as

$$M_y(x,t) = \exp(i\omega_e t)\sum_{r=7}^{\infty} p_r M_{yr}(x) \qquad (5)$$

where the modal internal actions along the ship, such as $M_{yr}(x)$ are evaluated from the 3D FE model according to the process described by Harding et al [21]. The variation of the amidships vertical bending, horizontal bending and twisting moment amplitudes with encounter frequency is shown in Figure 13. These variations reflect very closely the variations of p_7 for vertical bending moment, p_8 for horizontal bending moment and p_9 for torsional moment. This is because the contributions from higher distortional modes to the amidships wave-induced loads are small. Figure 13 illustrates the influence of tank filling scenarios on the predicted wave-induced loads.

5. CONCLUSIONS

A method for evaluating the interactions between liquid sloshing in partially filled tanks and hull motions and distortions has been developed and illustrated, for both symmetric and antisymmetric hull distortions, using an idealized LNG carrier stationary in beam waves and various partial filling scenarios.

The method is based on evaluating the added mass contributions due to liquid in partially filled tanks, using potential flow analysis and the Rankine de-singularised approach. The added mass coefficients associated with distortional modes, and their coupling to rigid body modes, were qualitatively assessed using three different partial filling scenarios. The method has also been verified using a partially filled tank with a flexible wall, whilst all other tank boundaries were rigid. The indications are that the method developed provides predictions whose trends can be explained physically.

The effect of sloshing in partially filled tanks is observed on the antisymmetric wave-induced loads, namely horizontal bending and torsional moments, predicted for the idealized LNG carrier stationary in beam regular waves at in the relatively small frequency range associated with ship-wave matching. No similar effects were observed on the vertical bending moment in beam regular waves. Furthermore, it was observed that these effects depend on the partial filling scenario, namely the position, as well as the dimensions, of the tank.

Further work should focus on more partial filling scenarios to confirm the behaviour of some distortional responses. A more realistic LNG carrier, with realistic filling scenarios and operations conditions, i.e. heading and forward speed should also be investigated.

7. ACKNOWLEDGEMENTS

The authors would like to thank Daewoo Shipbuilding & Marine Engineering, Co. Ltd. for their kind support.

8. REFERENCES

1. Kim, J.W., Lee, H. & Shin, Y. 'Sloshing impact load and strength assessment of membrane-type LNG containment system in large LNG carriers', *Proceedings of the 14th Offshore Symposium*, Houston, Texas, 2004.

2. Kim, Y. 'A numerical study on sloshing flows coupled with ship motion-The anti-rolling tank problem', *Journal of Ship Research*, 46, 52-62, 2002.

3. Rognebakke, O.F. & Faltinsen, O.M. 'Effect of sloshing on ship motions', *Proceedings of the 16th International Workshop on Water Waves and Floating Bodies (IWWWFB)*, Japan, 2001.

4. Kim, Y. 'Coupled analysis of ship motions and sloshing flows', *Proceedings of the 16th International Workshop on Water Waves and Floating Bodies (IWWWFB)*, Japan, 2001.

5. Nam, B., Kim, Y. & Kim, D. 'Nonlinear Effects of Sloshing Flows on Ship Motion', *Proceedings of the 21st International Workshop on Water Waves and Floating Bodies (IWWWFB)*, UK, 2006.

6. Malenica, S., Zalar, M. & Chen, X.B. 'Dynamic coupling of seakeeping and sloshing', *Proceedings of the 14th International Offshore and Polar Engineering Conference*, Hawaii, USA, 2003.

7. Newman, J.N. 'Wave effects on vessels with internal tanks', *Proceedings of the 20th International Workshop on Water Waves and Floating Bodies (IWWWFB)*, Norway, 2005.

8. Molin, B., Remy, F., Rigaud, S. & de Jouette, C. 'LNG-FPSOs: Frequency domain, coupled analysis of support and liquid cargo motions', *Proceedings of the 10th International Congress of the International Maritime Association of the Mediterranean (IMAM)*, Greece, 2002.

9. Nasar, T., Sannas, S.A. & Sundar, V. 'Experimental study of liquid sloshing dynamics in a barge carrying tank', *Journal of Fluid Dynamics Research*, 40, 427-458, 2008.

10. Lee, Y.B., Tan, M. & Temarel, P. 'Coupling between ship motion and sloshing using potential flow analysis', *Proceedings of the International Conference on Hydrodynamics*, France, 2008.

11. Lee, Y.B., Godderidge, B., Tan, M., Temarel, P., Turnock, S. & Cowlan, N. 'Coupling between ship motion and sloshing using potential flow analysis and rapid sloshing model', *Proceedings of the 19th International Offshore and Polar Engineering Conference*, Japan, 1, 54-62, 2009.

12. Lee, Y.B. 'Coupling between flexible ship and liquid sloshing using potential flow analysis', *PhD Thesis, University of Southampton*, 2010.

13. Graham, E.W. & Rodriguez, A.M. 'The characteristics of fuel motion which affect airplane dynamics', *Journal of Applied Mechanics*, 19, 381–388, 1952.

14. Godderidge, B., Turnock, S.R., Earl, C. & Tan, M. 'Identification of dangerous LNG sloshing using a Rapid Sloshing Model validated with computational fluid dynamics', *Proceedings of the 18th International Offshore and Polar Engineering Conference,* Vancouver, Canada, 2008.

15. Lee, Y.B., Tan, M., Temarel, P. & Miao, S.H. 'Coupling between flexible ship and liquid sloshing using potential flow analysis', *Proceedings of the 29th International Conference on Ocean, Offshore and Arctic Engineering (OMAE)*, Shanghai, China, OMAE2010-20787, 2010.

16. Lee, D.Y. 'A study on the sloshing of cargo tanks including hydroelastic effects', *PhD Thesis, Seoul National University*, 1997.

17. Kim, K.S., Kim, D.W., Lee, Y.B., Choi, S.H. & Kim, Y.S. 'Hydroelasticity vibration of a rectangular tank wall', *Proceedings of the ASME International Design Engineering Technical Conference*, California, USA, DETC2005-84222, 2005.

18. Bishop, R.E.D., Price, W. G. & Wu, Y. 'A general linear hydroelasticity theory of floating structures moving in a seaway', *Philosophical Transactions of the Royal Society London*, A 316, 375-426, 1986.

19. Leissa, A.W. 'Vibration of plates', *National Technical Information Service,* 1969.

20. Hirdaris, S.E., Price, W.G. & Temarel, P. 'Two-and three-dimensional hydroelastic modelling of a bulker in regular waves', *Marine Structures*, 16, 627–658, 2003.

21. Harding, R.D., Hirdaris, S.E., Miao, S.H., Pittilo, M. & Temarel, P. 'Use of hydroelasticity analysis in design', *Proceedings of the 4th International Conference on Hydroelasticity in Marine Technology*, China, 1-12, 2006.

9. AUTHORS BIOGRAPHY

Young Bum Lee obtained his PhD degree in 2010 at the University of Southampton. He currently works at Daewoo Shipbuilding & Marine Engineering, Co. Ltd. His expertise is in the area of fluid-structure interactions, especially sloshing.

Pandeli Temarel is Professor of Hydroelasticity at the School of Engineering Sciences, University of Southampton, and has extensive experience of fluid-structure interaction problems and, in particular, hydrodynamics, seakeeping, structural dynamics, hydroelasticity, manoeuvring and stability

Mingyi Tan is a lecturer in Ship Science at the University of Southampton. His research interests are in

the development and application of CFD and fluid-structure interaction.

Shihua Miao obtained his PhD degree at the University of Southampton in 1995. He has been working at the University of Southampton as a Research Fellow ever since. His expertise is in the areas of hydrodynamics, hydroelasticity and structural dynamics.

Mode (p, q)	Dry case Nastran	Wet Case		
		Nastran [17]	Kim et al [17]	Current method
(1, 1)	128.5	44.6	46.0	45.8
(2, 1)	152.6	91.7	93.1	93.0
(3, 1)	197.0	142.9	145.8	149.2
(4, 1)	262.7	181.9	194.2	211.4
(1, 2)	342.0	160.4	160.4	160.3

Table 1: Comparison of dry and wet natural frequencies of the flexible wall (Hz) obtained from various methods; 50% filling level for the wet case

Ship length (m)	315
Ship breadth (m)	50
Ship depth (m)	27
Ship draft (m)	8.8
Tank breadth (m)	44
Displacement (tonnes)	142500

Table 2: Main particulars of the idealized LNG carrier

Mode	Tank 1 (or 3) T=20m	Whole Ship T=20m
Longitudinal (m=0)	0.61	0.14
Longitudinal (m=1)	1.21	0.4
Longitudinal (m=2)	1.56	0.61
Transverse (n=0)	0.79	0.79
Transverse (n=1)	1.45	1.45
Transverse (n=2)	1.87	1.87
Diagonal (m=0, n=0)	0.90	0.8
Diagonal (m=1, n=0)	1.27	0.83
Diagonal (m=0, n=1)	1.47	1.45

Table 4: Sloshing natural frequencies (rad/s) for tank 1 or 3 (scenarios A and B) and the whole ship filled with liquid (scenario C), obtained from equation 3

Mode	ω_r
r=7 (2 node VB)	0.55
r=8 (2 node HB)	0.91
r=9 (1 node T)	1.12
r=10 (3 node VB)	1.32
r=11 (3 node HB)	1.91

Table 3: Dry hull natural frequencies ω_r (Hz) of the idealized LNG carrier; VB: Vertical bending, HB: Horizontal bending, T: Twisting

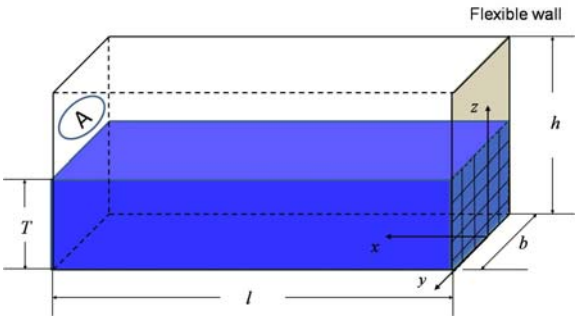

Figure 1: A rectangular tank with a flexible wall used by Lee, and Kim et al [16, 17]

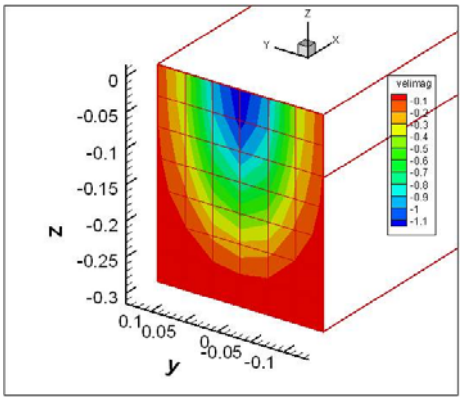

Figure 2: Velocity distribution for 1st dry mode (1, 1) on the submerged part of the wall

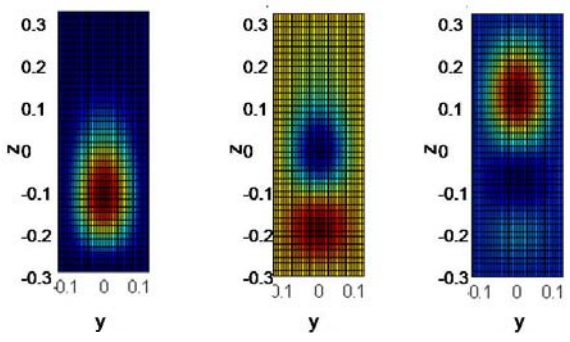

Figure 3: First few wet mode shapes of the flexible submerged wall - identified using the dry mode (p, q)

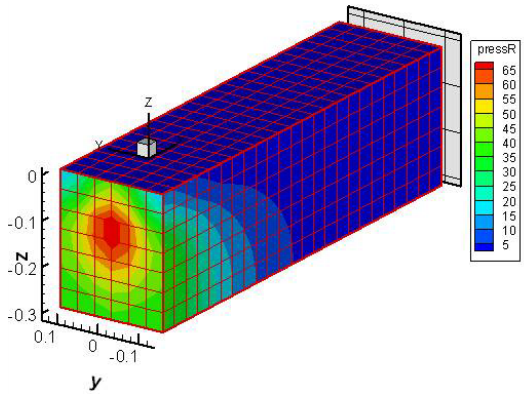

Figure 4: Pressure distribution for 1st (wet) mode on the submerged flexible wall, when zero potential free surface boundary condition is applied

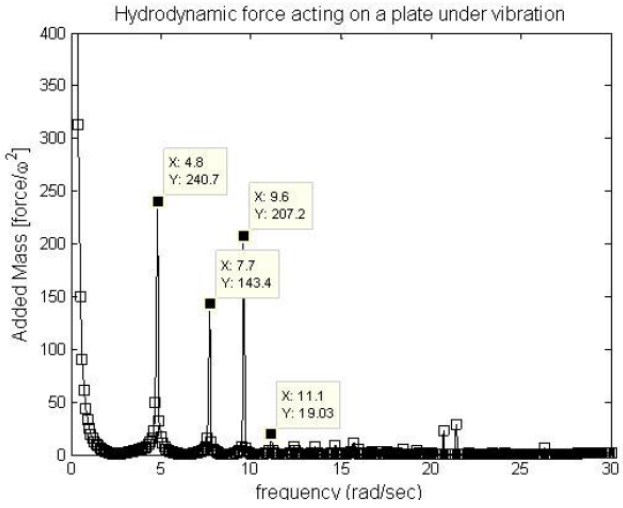

Figure 5: Generalised added mass for the 1st (wet) mode shape, using the free surface boundary condition of equation 1

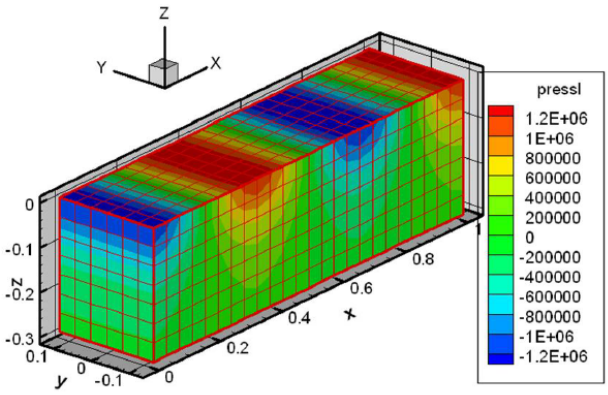

Figure 6: Pressure distribution for 1st (wet) mode of the submerged flexible plate wall, using the free surface boundary condition of equation 1; excitation frequency is 9.6 rad/s, i.e. 2nd antisymmetric sloshing mode

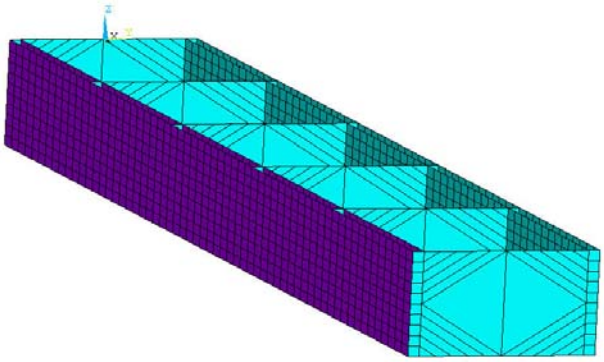

Figure 7: FE model of the idealized LNG Carrier; axis system at AP; tanks numbered as 5, 4, 3, 2, 1 from AP

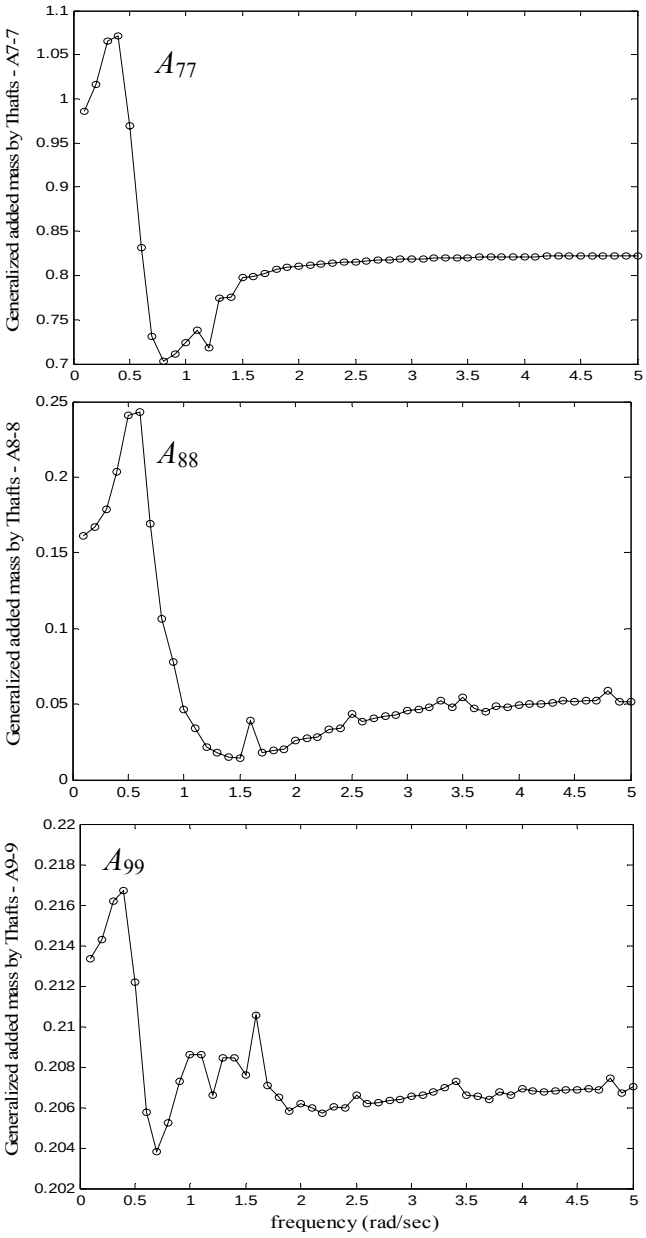

Figure 8: Selection of generalized added mass variations, for global distortional modes (A_{77}, A_{88}, A_{99}), with frequency for the LNG carrier oscillating in water (uncoupled problem)

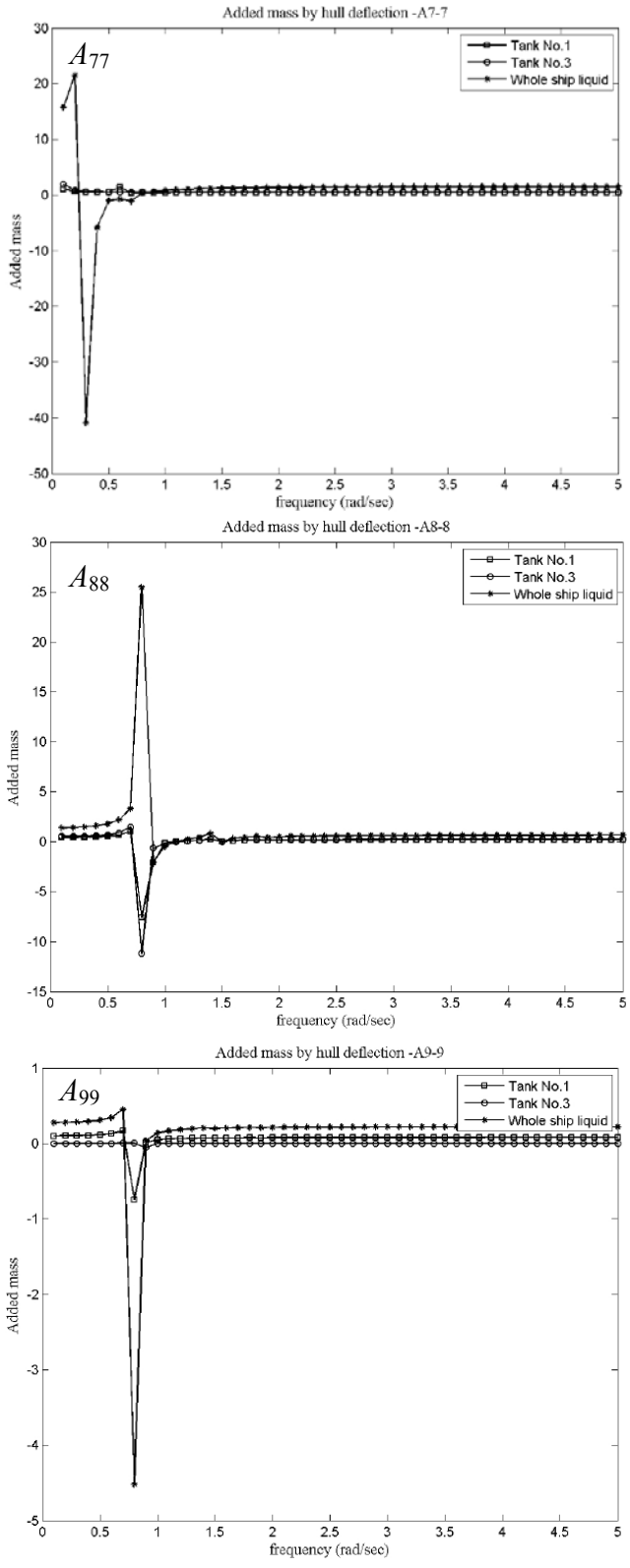

Figure 9: A selection of generalised added mass coefficients, for distortion modes (A_{77}, A_{88}, A_{99}) due to sloshing inside the partially filled tank(s)

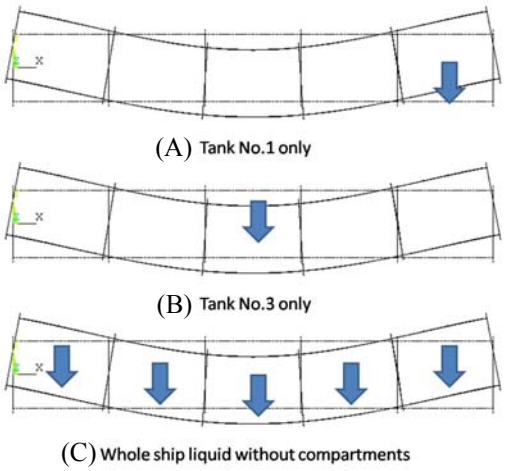

Figure 10: Tank arrangement and explanation of the influence of sway for the generalised added mass coefficients shown in Figure 11

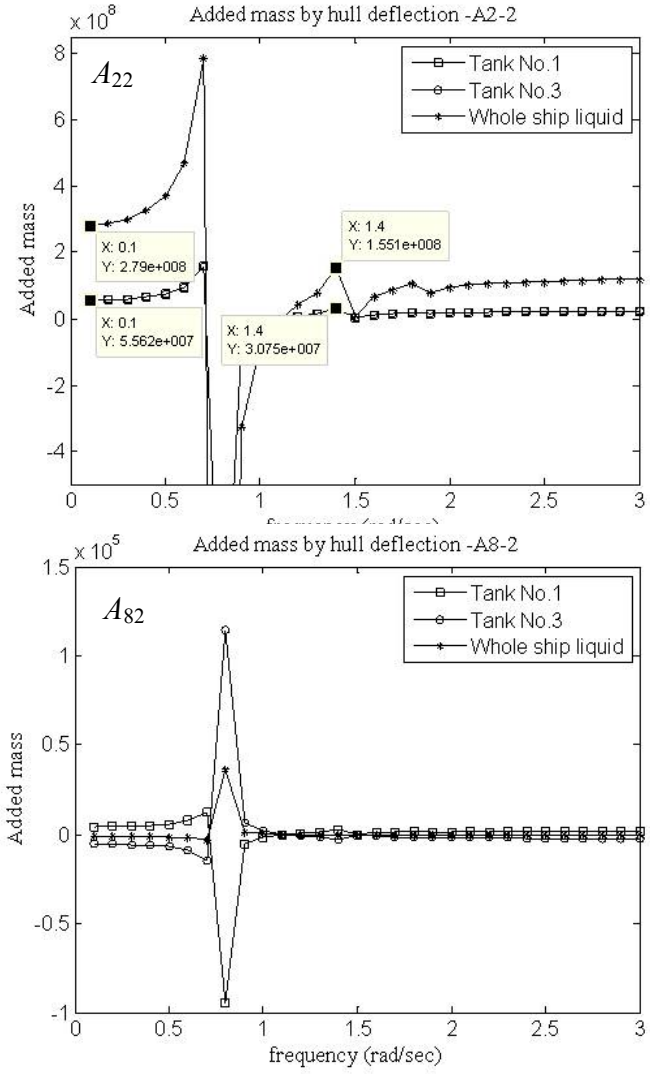

Figure 11: Illustration of the influence of sway coupling on generalised added mass coefficients A_{22} and A_{82}

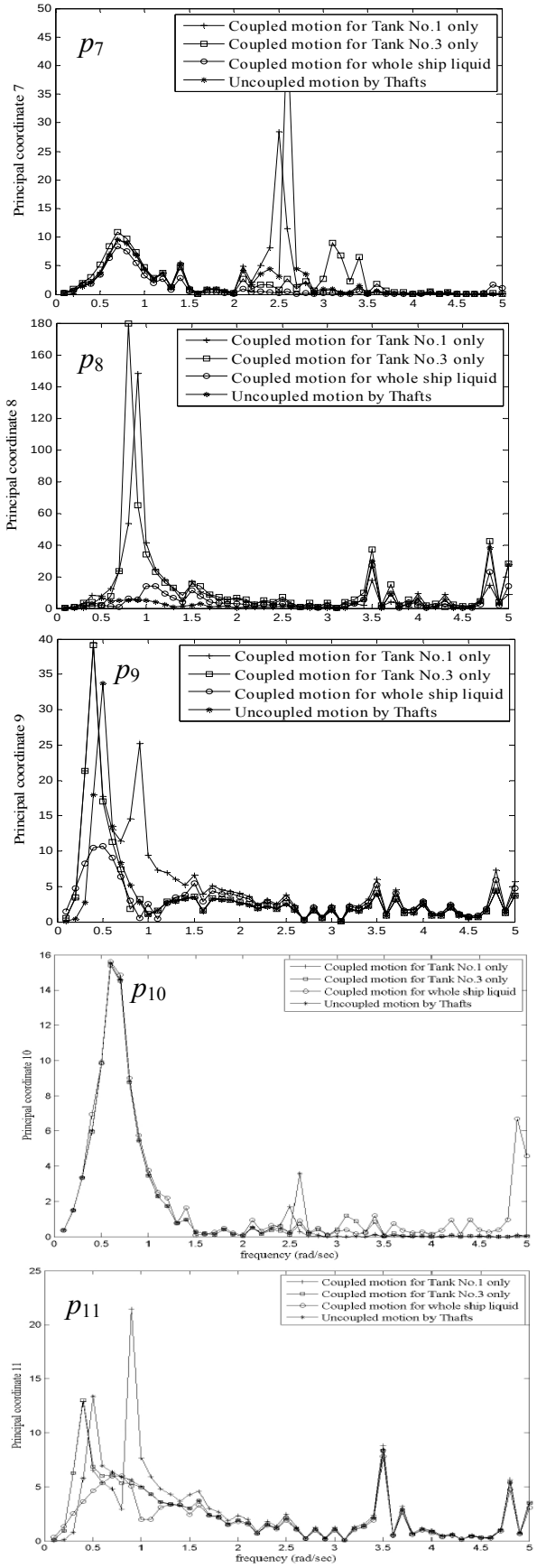

Figure 12 Variation of principal coordinates for the LNG carrier stationary in regular beam waves, illustrating the influence of liquid sloshing with different configurations

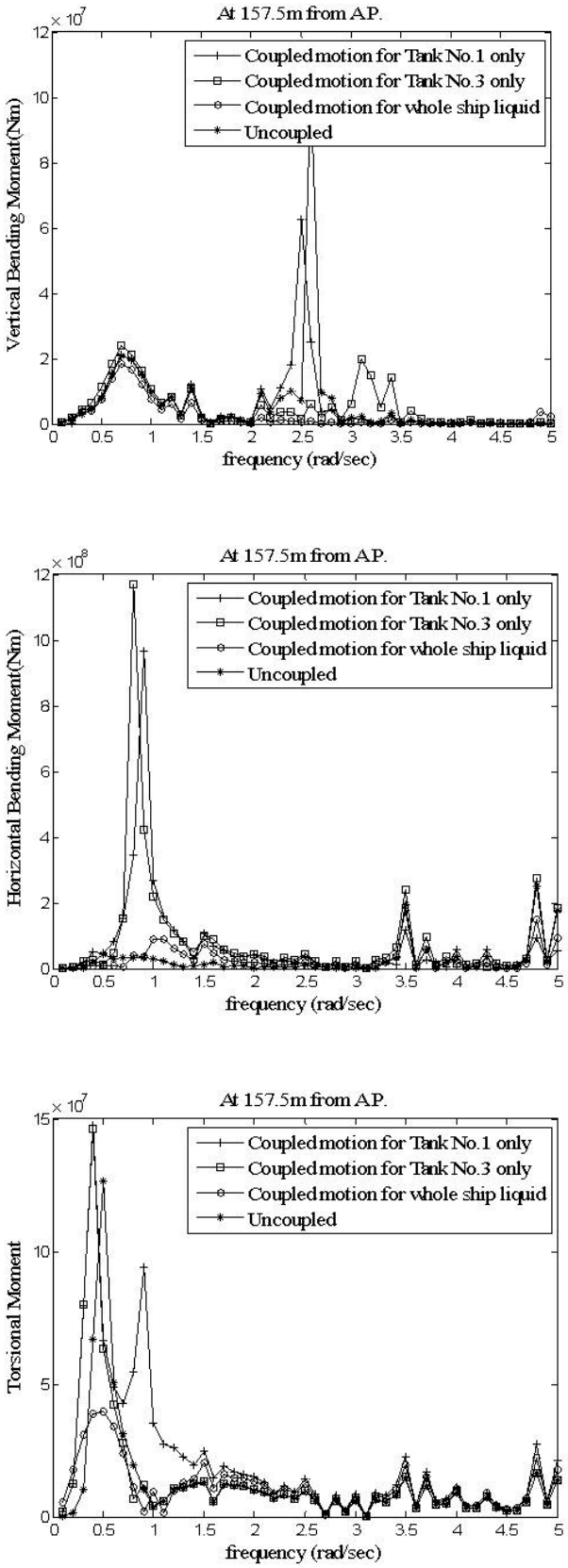

Figure 13: Variation of amidships wave-induced vertical bending, horizontal bending and torsional moments for the LNG carrier stationary in regular beam waves, illustrating the influence of liquid sloshing with different configurations